JTTEE5 14:342-353
DOI: 10.1361/105996305X59387
1059-9630/$19.00 © ASM International

Peer Reviewed

Inclusion of Aerodynamic Non-Equilibrium Effects in Supersonic Plasma Jet Enthalpy Probe Measurements

A. Blais, B. Jodoin, J-L. Dorier, M. Gindrat, and C. Hollenstein

(Submitted July 12, 2004; in revised form September 30, 2004)

Low pressure plasma spraying (LPPS) is a thermal spraying technique that has found a niche for low oxidation products. It uses a low pressure environment (i.e., chamber pressure between 2 and 90 kPa) and yields supersonic plasma jets. The enthalpy probe technique is a common measurement method in plasmas. However LPPS jets are difficult to diagnose as their supersonic nature forces the apparition of a shock wave in front of any measuring device inserted in the jet. Incomplete or erroneous assumptions are usually invoked to overcome the difficulties associated with this shock wave and carry out the LPPS jet diagnosis from enthalpy probe measurements. In this work, a new device is designed to gain access to an additional physical quantity, which is needed to assess the aerodynamic non-equilibrium state of the jet. It is combined with enthalpy probe measurements, and the resulting set of experimental data is used with a numerical procedure based on gas dynamics theory, yielding free-stream supersonic plasma jet values from the measurements behind the induced shock wave. The results agree well with the phenomenology of supersonic jets in aerodynamic nonequilibrium. However this new method is restricted by the local thermodynamic equilibrium assumption, which is directly linked with the pressure and temperature conditions of the plasma jet.

Keywords enthalpy probe, low pressure plasma spray, modeling, supersonic plasma

1. Introduction

Thermal spraying is a worldwide growing industry, worth billions of dollars annually, and has become an important part of the materials processing industry (Ref 1, 2). It consists of the deposition of a metallic or ceramic coating providing new characteristics to a substrate. These new characteristics can be improved resistance to heat, wear, corrosion, abrasion, erosion or oxidation, a change in electrical properties, or even a dimensional restoration (Ref 1-6). Plasma spraying techniques generally rely on two possible plasma sources, namely the direct current (dc) and radiofrequency (rf) plasma torches. From a scientific perspective, the choice of the source depends mainly on the requirements of the sprayed material, such as the melting temperature, the in-flight residence time and the speed upon impact. Low pressure plasma spraying (LPPS), also termed vacuum plasma spraying (VPS), was developed in the early 1970s. It uses plasma torches equipped with a *de Laval* nozzle[1] inside a low-pressure chamber (Ref 8); hence the plasma exits the torch at supersonic velocities. For spraying purposes, the supersonic low-pressure plasma jet is seeded with particles that are accelerated and melted before impacting the substrate. A secondary gas with high enthalpy and thermal conductivity is often used in plasma spraying to enhance melting of the injected particles. The result is a high-quality, high-density coating with excellent bonding and cohesive strength (Ref 1, 4). The controlled environment also has the advantage of lowering the oxidation of

A. Blais and **B. Jodoin,** Faculty of Engineering, University of Ottawa, 161 Louis-Pasteur, Ottawa, ON, Canada; and **J-L. Dorier, M. Gindrat,** and **C. Hollenstein,** Swiss Federal Institute, CRPP, Station 13, CH-1015 Lausanne, Switzerland. Contact e-mail: jodoin@genie.uottawa.ca.

[1]The *de Laval* nozzle is a converging-diverging nozzle named after the Swedish engineer Carl Gustaf Patrik de Laval (1845-1913), who used such a nozzle in steam turbines from 1883 (Ref 7). de Laval officially presented his steam turbine at the 1893 Chicago Colombian Exposition.

Nomenclature

c	speed of sound, m/s
c_p	specific heat at constant pressure, J/(kg K)
c_v	specific heat at constant volume, J/(kg K)
h	enthalpy, J/kg
$\dot{m}_{gas}$	gas mass flow rate, kg/s
$\dot{m}_w$	cooling water mass flow rate, kg/s
M	Mach number, 1
p	static pressure, Pa
p_c	chamber pressure, Pa
p_e	torch exit pressure, Pa
p_o	stagnation pressure, Pa
R	specific gas constant, J/(kg K)
s	entropy, J/(kg K)
S_{sw}	shock generated entropy, J/(kg K)
T	static temperature, K
T_o	stagnation temperature, K
T_w	cooling water temperature, K
v	velocity, m/s
z	axial location, m
γ	specific heat ratio, 1
ρ	density, kg/m^3
$( )_s$	isentropic process ($ds = 0$)

the sprayed material, which enables a better control of the coating composition and morphology. This reflects through a greater structural homogeneity, an absence of oxides, and hardness improvement (Ref 1, 4). The drawback of an LPPS system is mainly its elevated initial and operational costs, as it requires a closed chamber with an efficient pumping unit to achieve the desired conditions of controlled atmosphere. Thus LPPS is mainly used for the production of coatings with a high added value.

The development and optimization of LPPS processes are dependent upon knowledge of the involved physics. However, a complete process characterization based on measurements is highly demanding, if not an unreachable objective. Therefore, the use of theoretical models is prescribed. To be useful for understanding the encountered phenomena, these models have to be validated with measurements. In addition to the difficulties pertaining to any thermal spray process, LPPS measurements are further complicated by the supersonic nature of the plasma jet, which might lead to aerodynamic and/or chemical nonequilibrium. These measurements are carried out using an intrusive technique (i.e., an enthalpy probe) to obtain the temperature and velocity of the plasma jet. As the jet is supersonic, a natural mechanism (i.e., a shock wave) slows it down at the tip of the probe. This shock abruptly changes the properties of the plasma jet by increasing both its temperature and pressure, making it difficult to link the measurements with the free-stream plasma jet values.

This paper is devoted to explaining and solving problems encountered with enthalpy probe measurements in supersonic plasma jets. First, an enthalpy probe measurement review highlighting the specific problems in supersonic flows is carried out. From a brief overview on the characteristics of supersonic flows, the major problems pertaining to the measurement and physical interpretation of such flows are presented. Second, a new method to interpret supersonic enthalpy probe measurements is described, eluding the preceding problems. Third, the experimental setup and the results are presented, followed by a discussion of the supersonic free-stream plasma jet characteristics obtained from the new method. Finally, conclusions are drawn from the results of the new method.

2. Enthalpy Probe Measurements Review

The development of the enthalpy probe in its current form is attributed to Grey et al. in the 1960s (Ref 9, 10). Miniaturization of the high pressure water-cooled probe was realized by Greyrad Corporation and then commercialized by Calprobe under patent license from Grey (as cited in Ref 11).

The early works on enthalpy probe diagnostics were concerned with the elaboration of different types of thermodynamic probes to establish a convenient and reliable measurement method. This led to the development and testing of single-jacketed probes (Ref 9, 10, 12, 13), double-jacketed probes (Ref 9, 11-13) and fast-response uncooled probes (Ref 12, 14). The single-jacket enthalpy probe was retained as an effective, simple, and low-cost technique.

The first studies on thermal plasmas using enthalpy probes dealt with laminar and turbulent mixing in jets (Ref 15-17). Supersonic plasma jets with probe-attached shock waves and jet

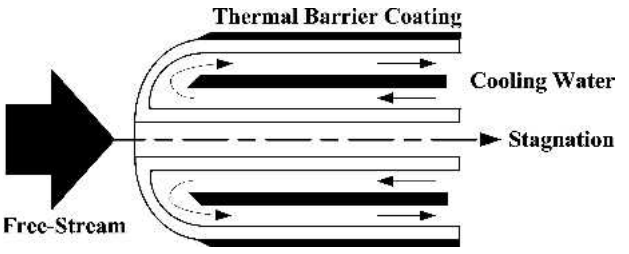

Fig. 1 Schematic illustration of an enthalpy probe

swallowing, an alternative to the common detached-shock blunt-nose enthalpy probe, were studied (Ref 18). Studies on ambient gas entrainment and onset of turbulence for atmospheric plasma jets were also conducted (Ref 19, 20), as well as a work addressing the specificities of an argon jet discharging in a controlled argon atmosphere (Ref 21). Combining a mass spectrometer to the enthalpy probe system allowed to assess the presence of demixing inside the plasma jet mixture (Ref 22, 23). The enthalpy probe measurement technique was applied to compressible plasma jets (Ref 24) and more specifically to supersonic plasma jets (Ref 25). It was also compared with other plasma measurement techniques such as laser-doppler anemometry (LDA), emission spectroscopy, coherent antistokes raman spectroscopy (CARS), and laser light scattering (Ref 20, 26). A review on the use of enthalpy probes in thermal plasmas can be found in Ref 27.

The aim of the present work is to propose a solution for enthalpy probe measurements of supersonic plasma jets overcoming the incompleteness of supersonic flow analysis found in the literature. Hence it requires to show the provenance and working principles of enthalpy probes and to detail the peculiarities pertaining to supersonic flows. These details and explanations are mandatory as they provide a logical way to expose the new method for enthalpy probe measurements in supersonic plasma jets.

2.1 Enthalpy Probe

The enthalpy probe is similar to a water-cooled Pitot tube with no circumferential pressure tap, as shown in Fig. 1. Primarily developed to deduce the temperature of a high-energy flow from enthalpy measurements, the enthalpy probe can also be used to infer the velocity of high-energy flows if the flow static pressure is known.

Enthalpy measurements are carried out comparing the cooling water temperature increase ΔT_w in two different cases: tare and sample. The former case is the condition of no-flow through the probe, while in the latter case a known flow rate of gas is collected by the probe. Nowadays, enthalpy probes are often covered with a thermal barrier coating (TBC), which provides a larger heat load difference between the tare and sampling modes, improving the quality of enthalpy measurements (Ref 27, 28).

From an energy balance on the cooling water circuit, the plasma temperature is deduced (using LTE assumptions) from the enthalpy of the high-energy jet $h_{unknown}$ (Ref 10):

$$\dot{m}_{gas}(h_{unknown} - h_{exit}) = (\dot{m}_w c_p{}^w \Delta T_w)_{sample} - (\dot{m}_w c_p{}^w \Delta T_w)_{tare} \quad \text{(Eq 1)}$$

In Eq 1, $\dot{m}_{gas}$ is the mass flow rate of gas into the probe, h_{exit} is the enthalpy of the gas leaving the probe, $\dot{m}_w$ is the cooling water mass flow rate, c_p^w is the cooling water specific heat at constant pressure and $\Delta T_w = (T_w^{out} - T_w^{in})$ is the cooling water temperature rise. The quantities ΔT_w, $\dot{m}_w$, and $\dot{m}_{gas}$ are all measured, while h_{exit} is usually neglected.

2.2 Incompressible Jet Velocity Measurements

The incompressible flow regimen is encountered for $M < 0.3$, where the Mach number ($M = v/c$) is the ratio of the flow velocity (v) to the speed of sound in the fluid ($c = (\sqrt{\partial p/\partial \rho})_s$). Pitot tubes are effective velocity measurement devices for incompressible low-energy jets. In that case, v is found using the Bernoulli equation (i.e., an energy balance for a steady, adiabatic, workless, incompressible fluid flow):

$$v = \sqrt{\frac{2(p_o - p)}{\rho}} \qquad \text{(Eq 2)}$$

The subscript "o" denotes the stagnation point of the flow (i.e., zero velocity).

Dealing with high-energy (i.e., with chemical reactions such as dissociation, ionization, and recombination) incompressible jets, the Pitot tube can still be used provided that the flow temperature (T) is known, allowing to find the density (ρ), and that the probe is able to sustain the heat flux of the impacting stream without any damage. These requirements are met by a water-cooled enthalpy probe. For incompressible jets, the static pressure of the high-energy flow (p) is the ambient or chamber pressure (p_c).

2.3 Subsonic Jet Velocity Measurements

If the Mach number is in the range $0.3 \leq M \leq 1$, the flow is in the subsonic regimen. For such a flow, the Bernoulli equation does not apply anymore. To take compressibility effects in consideration, the one-dimensional energy equation written between the free-stream and stagnation points in the jet is used and combined to the stagnation-to-static temperatures ratio. Then, assuming the working gas to be calorically perfect (c_p = constant and $p = \rho R T$), the enthalpy change is given by $\Delta h = c_p \Delta T$, the specific heat ratio is $\gamma = c_p/c_v$ and the gas constant is $R = c_p - c_v$. Combining these definitions, the velocity (v) is obtained as (Ref 29):

$$v = \sqrt{\frac{2\gamma R T}{\gamma - 1}\left[\left(\frac{p_o}{p}\right)^{\frac{\gamma}{\gamma-1}} - 1\right]} \qquad \text{(Eq 3)}$$

Hence to compute the velocity of a compressible subsonic jet, the stagnation pressure p_o, the static pressure p, and the temperature T must be known.

2.4 Supersonic Jets

In the supersonic regimen ($M > 1$), the flow travels faster than the speed of sound in the fluid, which leads to a completely different behavior. Theoretical grounds of supersonic jets are exposed to highlight common incorrect enthalpy probe measurement interpretations from the one-dimensional isentropic description of an ionized gas.

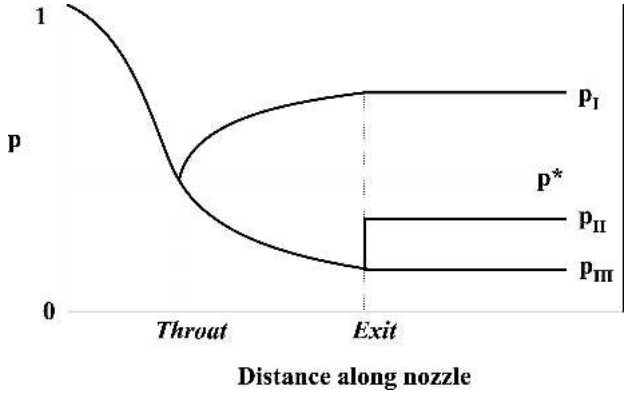

Fig. 2 Pressure distributions inside a de Laval nozzle (p^* is the pressure at the minimum area where $M^* = 1$)

2.4.1 Supersonic Flow Generation. In a dc plasma torch, the gas stream is confined between the outer anode and the central cathode. Reducing the exit area of the torch (i.e., converging nozzle) increases the velocity at constant mass flow rate. Decreasing the chamber pressure (p_c) also accelerates the flow until the maximum mass flow rate is attained, for which $M = 1$ (Ref 29). Further decreasing p_c will not increase the mass flow rate: the converging nozzle is choked. As the supersonic flow velocity increases in a diverging section (Ref 29), a de Laval nozzle must be used[2] for the flow to reach higher velocities (i.e., $M > 1$).

Figure 2 illustrates the possible pressure distributions inside the de Laval nozzle when p_c is varied. They can be regrouped to represent different physical behaviors of the jet as p_c is lowered. Starting from no flow condition, p_c is decreased until the flow attains the subsonic regimen. When $p_c = p_I$, sonic flow is reached at the throat of the nozzle ($M_{throat} = 1$), the converging section is choked, and the flow stays subsonic in the diverging section. For the pressure range $p_I > p_c > p_{II}$, the flow becomes supersonic with a shock wave forming inside the nozzle, progressing from throat to exit as p_c decreases. When $p_c = p_{II}$, a shock wave is formed exactly at the exit of the nozzle. As $p_{II} > p_c > p_{III}$, shock waves are forming outside the nozzle (i.e., overexpanded jet). For $p_c = p_{III}$, the flow is supersonic and shockless (i.e., aerodynamic equilibrium). Finally when $p_c < p_{III}$, the flow is supersonic with expansion waves forming outside the nozzle (i.e., underexpanded jet).

2.4.2 Shock Waves and Aerodynamic Non-Equilibrium in Supersonic Flow. A shock wave is a discontinuity created from the coalescence of pressure waves forming a sharp front. It is an irreversible process characterized by viscous and heat conduction phenomena that converts the flow kinetic energy into thermal energy, raising its temperature and pressure (Ref 29).

External shock solutions (i.e., over- and underexpanded jets)

[2]The rf plasma torch, which consists of a cylindrical glass tube surrounded by an electromagnetic coil, can also be used in combination with a de Laval nozzle to achieve supersonic velocities (Ref 25, 30).

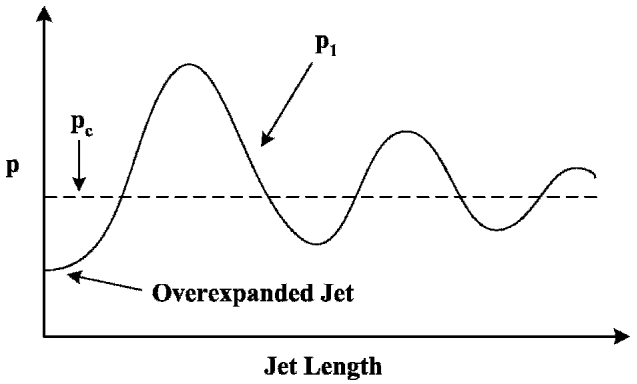

Fig. 3 Axial free-stream static pressure of a supersonic jet in aerodynamic nonequilibrium (overexpanded jet shown; p_c is the chamber pressure and p_1 the free-stream jet static pressure)

represent aerodynamic nonequilibrium of the flow where the jet static pressure at torch exit (p_e) differs from the chamber pressure (i.e., $p_e \neq p_c$). This inequality brings an oscillatory pressure pattern, as shown in Fig. 3, caused by expansion and compression waves that readjust the flow for the jet static pressure to reach p_c.

2.4.3 Supersonic Jet Velocity Measurements. To obtain the velocity of a supersonic flow, Eq 3 cannot be used because of the appearance of a shock wave in front of the measurement device. Two different states are to be accounted for when using a probe inside a supersonic jet. As shown in Fig. 4 and 5, these states are located on both sides of the shock wave (before = 1, after = 2).

If the gas is calorically perfect and the flow between the shock wave and the probe is one-dimensional, steady, isentropic, and workless, the following relationships apply (Ref 29):

$$\frac{T_o}{T} = 1 + \frac{\gamma - 1}{2} M^2 \qquad \text{(Eq 4)}$$

$$\frac{p_o}{p} = \left(1 + \frac{\gamma - 1}{2} M^2\right)^{\frac{\gamma}{\gamma - 1}} \qquad \text{(Eq 5)}$$

Combining Eq 4 and 5 yields:

$$\frac{p_{o2}}{p_1} = \left[1 + \frac{\gamma - 1}{2}\left(\frac{M_1^2 + \frac{2}{\gamma - 1}}{\frac{2\gamma}{\gamma - 1} M_1^2 - 1}\right)\right]^{\frac{\gamma}{\gamma - 1}} \left(\frac{2\gamma M_1^2 - \gamma + 1}{\gamma + 1}\right) \qquad \text{(Eq 6)}$$

Solving Eq 6 requires knowledge of the jet stagnation pressure after the shock p_{o2}, the jet static pressure before the shock p_1 and the jet temperature T (to evaluate γ). In the special case of aerodynamic equilibrium ($p_e = p_c$), p_1 is known ($p_1 = p_c$), and enthalpy probe measurements give access to p_{o2} and h_{o2}. The calorically perfect gas assumption is also required for γ to be constant. When the preceding requirements are met, the free-stream jet velocity v_1 is found from Eq 6 and from the

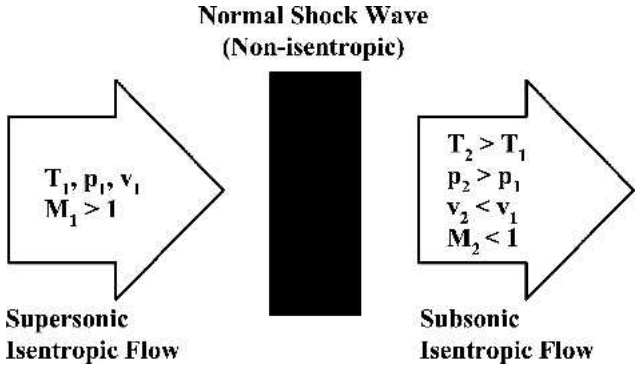

Fig. 4 Normal shock wave in a one-dimensional, isentropic flow

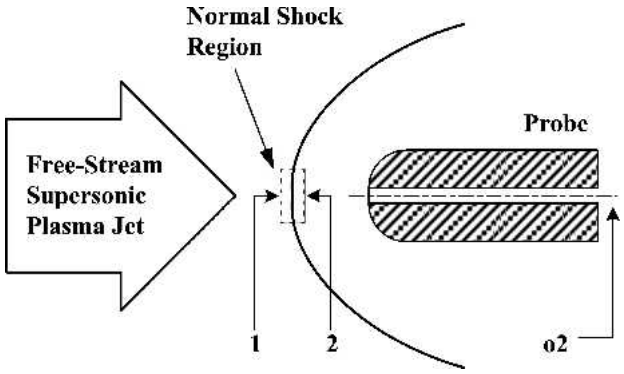

Fig. 5 Normal shock wave formation from the insertion of a measuring device inside a supersonic jet

evaluation of the speed of sound in the free-stream plasma jet c_1 ($c_1 = v_1/M_1$).

2.5 Supersonic Plasma Jet Enthalpy Probe Measurements: Common Interpretation and Related Problems

This section presents the common approach found in the literature to interpret enthalpy probe measurements in supersonic plasma flows (Ref 24, 25, 27).

2.5.1 Common Interpretation. Equation 6 is solved to yield the free-stream plasma jet Mach number M_1 by assuming that the gas is calorically perfect (i.e., γ is constant through the evolutions between states 1, 2, and o2). From the energy conservation law, the definitions of the Mach number, the velocity of sound in a calorically perfect gas applied to the free-stream plasma jet:

$$h_1 + \frac{v_1^2}{2} = h_{o1} = h_{o2} \qquad \text{(Eq 7)}$$

$$v_1 = M_1 c_1 \qquad \text{(Eq 8)}$$

$$c_1 = \sqrt{\gamma R T_1} \qquad \text{(Eq 9)}$$

Equations 7-9 can be rearranged as:

$$h_1 = h_{o2} - M_1^2 \frac{\gamma R T_1}{2} \quad \text{(Eq 10)}$$

where h_{o2} (from measurements) and M_1 (from Eq 6 solved with the assumption that $p_1 = p_c$) are known. Equation 10 is iteratively solved using thermodynamic tables of the working plasma gas, simultaneously obtaining T_1 and h_1. It must be noted that the specific heat ratio γ and the gas constant R are both functions of temperature and pressure. The velocity v_1 is found using equations 8 and 9 while the density ρ_1 is computed from the perfect gas law $\rho = p/(RT)$. Hence all the free-stream plasma jet properties are found from isentropic gas dynamics theory for a calorically perfect gas assuming aerodynamic equilibrium.

2.5.2 Problems Related to the Common Interpretation. Theoretical efforts were presented in Sec. 2.5.1 to infer the supersonic plasma jet free-stream properties from the stagnation quantities measured using an enthalpy probe. With Eq 6 linking both sides of the shock wave appearing in front of the probe, two major problems arise.

First, as the temperature is high enough for ionization to occur, the gas cannot be considered calorically perfect as the values of c_p and γ change along with temperature and pressure. Thus discrepancies are found between the different γs of Eq 6 (i.e., Eq 6 has two steps: the shock wave, from 1 → 2, and the stagnation, from 2 → o2). Due to these considerations, Eq 6 should be seen as $p_{o2}/p_1 = f(M_1, \gamma_1, \gamma_2, \gamma_{o2})$, where the different γs expose a difficulty in working with Eq 6. In fact, all the one-dimensional isentropic equations were developed for calorically perfect gases (Ref 29): their use with thermal plasmas bring unavoidable errors.

Secondly, as typical LPPS operating conditions deal with over- and underexpanded jets for which the axial free-stream static pressure distribution (p_1) displays an oscillating behavior, the plasma jet is not in aerodynamic equilibrium. Thus, p_1 cannot be directly measured due to the shock wave forming in front of any measurement device inserted in the supersonic plasma jet, preventing the solution of Eq 6 and 10. However, it was shown that p_1 and M_1 could be obtained from a tedious numerical jet study (Ref 31, 32).

Consequently, most LPPS flows are neither in aerodynamic equilibrium ($p_1 \neq p_c$) nor calorically perfect ($c_p \neq$ constant), preventing the use of Eq 6. To overcome these problems about p_1 and γ with supersonic plasma jets, it is often assumed that (Ref 24, 25, 27) $p_1 = p_c$ even if the jet is not in aerodynamic equilibrium, and the flow is frozen, i.e., the hydrodynamic timescale is smaller than the chemical timescale and thus c_p and γ are constant.

As detailed in Fig. 3 and in Ref 33, the aerodynamic nonequilibrium cannot be neglected as the use of $p_1 = p_c$ in overexpanded jets lead to a large overestimation on the velocity profile. Furthermore, even if the frozen flow assumption is achievable in a supersonic plasma jet, it might not hold in the region behind a shock wave where the flow is slowed down with its temperature and pressure increased, three conditions promoting chemical equilibrium inside an aerodynamic nonequilibrium flow (Ref 34).

Taking into consideration the preceding difficulties with supersonic flow measurements in plasma jets, a new method is tailored to infer free-stream supersonic plasma jet properties in the next section without having to use the assumption of a calorically perfect gas in aerodynamic equilibrium.

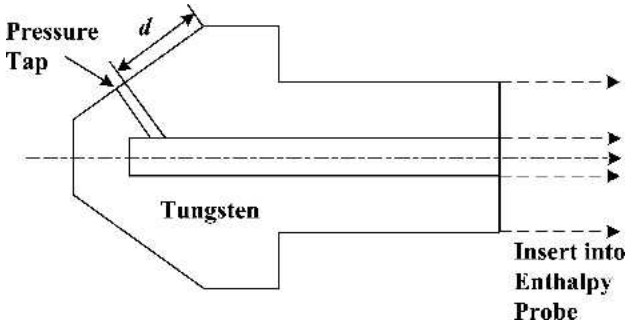

Fig. 6 Schematic illustration of the PSSPP

3. New Method for Enthalpy Probe Measurements of Supersonic Plasma Jets in Aerodynamic NonEquilibrium

To avoid the pitfalls presented in the previous section, a new method is developed and detailed (Ref 33). A procedure is used to infer the plasma jet values before the shock, using a new device to gain access to the static pressure after the shock (p_2), as detailed in section 3.1. The conservation equations governing the normal shock wave process are presented in section 3.2. The solution procedure is discussed in section 3.3.

3.1 Post-Shock Static Pressure Probe

The post-shock static pressure probe (PSSPP) consists of a conical truncated piece of tungsten with a pressure tap located on its surface, as shown in Fig. 6. It is fixed as a cap on the tip of an enthalpy probe. A detached shock forms in front of the PSSPP, and the resulting flow is parallel to the conical surface. The idea behind the PSSPP design is allowing the flow to recover the pressure it had just after undergoing the shock wave as it reaccelerates on the PSSPP surface. Consequently the pressure tap measures the static pressure (p_2) of the plasma jet after the shock. Numerical simulations were conducted to describe the flow reacceleration on the PSSPP conical surface (Ref 33), and the results are presented as iso-pressure contours in Fig. 7, where p_2 is found on the PSSPP surface during the reacceleration. These simulations were used to obtain the location of the tap for a meaningful p_2 to be measured (i.e., fixing the value of d on Fig. 6).

It is critical to establish a similarity between the PSSPP- and probe-induced shocks. If both shocks have similar shapes and magnitudes, it allows combination of PSSPP and stagnation measurements. Two indicators of shock similitude are obtained by comparing the standoff distances between the shock front and the tip of the intrusive measurement tools (probe and PSSPP) and by comparing the stagnation pressures (p_{o2}) measured with the probe and with the PSSPP. Figure 8 presents two pictures of the supersonic plasma jet impinging the enthalpy probe and the

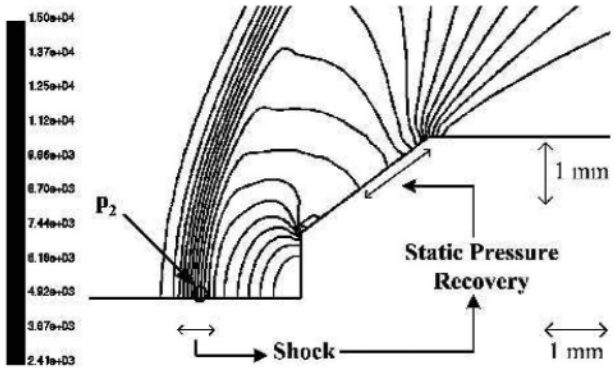

Fig. 7 Static pressure recovery from the reacceleration of the flow on the PSSPP surface (M = 1.5, p = 4000 Pa, and T = 1000 K)

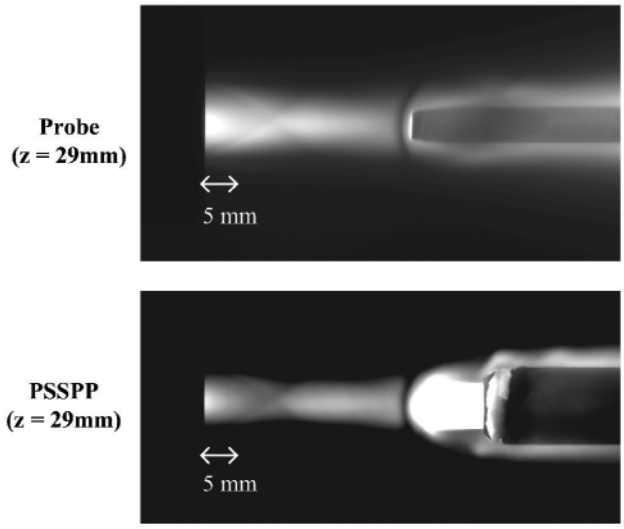

Fig. 8 Shock/measuring device distances; both devices are located 29 mm downstream of torch exit (top: enthalpy probe, bottom: PSSPP)

PSSPP at a distance of 29 mm from the torch exit. Under the same free-stream plasma jet conditions, the normal shocks and ensuing subsonic flows are similar, as indicated by the constant shock-tool distance of approximately 2 mm, which implies from gas dynamics considerations that $p_{2\text{-probe}} \approx p_{2\text{-PSSPP}}$. It should be noted that the plasma jet looks different in the two parts of Fig. 8 as different filters were used on the charge-coupled device (CCD) camera to account for the bright reemission of the incandescent PSSPP. The correspondence between the stagnation pressures p_{o2} obtained from enthalpy probe measurements and from PSSPP measurements was also verified using a specially designed PSSPP (i.e., with a hole at its tip).

3.2 Normal Shock Equations

The assumptions to describe the normal shock wave process require that the shock is thin and of constant area and the flow is one-dimensional, steady, adiabatic, and workless. Furthermore, the chamber pressure and the jet temperature must provide enough collisions (i.e., relatively small mean free path and large number density) for the ionized gas to be above the continuum limit. Under these conditions, the conservation equations describing the flow on both sides of the shock (Fig. 4 and 5) are:

- Mass: $\rho_1 v_1 = \rho_2 v_2$ (Eq 11)
- Momentum: $p_1 + \rho_1 {v_1}^2 = p_2 + \rho_2 {v_2}^2$ (Eq 12)
- First Law of Thermodynamics: $h_1 + \frac{{v_1}^2}{2} = h_2 + \frac{{v_2}^2}{2}$ (Eq 13)
- Second Law of Thermodynamics: $s_2 = s_1 + S_{sw}$ (Eq 14)
- State: $p = \rho R T$ (Eq 15)

To solve the system of equations describing the shock wave (Eq 11-13) and to obtain the free-stream properties of the flow at location 1, three measurements are required after the shock wave. Different sets are possible depending on the variables that can be measured. In this work, those values are the static pressure p_2, the stagnation pressure p_{o2}, and the stagnation enthalpy h_{o2}; the latter two are from enthalpy probe measurements while the former is obtained using the PSSPP. With p_2, p_{o2}, and h_{o2} known, the conservation equations are solved to obtain the properties of the free-stream supersonic plasma jet, as discussed in the following section.

3.3 Solution Method

With h_{o2}, p_{o2}, and p_2 measured, it is possible to carry out the calculation of all the plasma stream variables at location 2, namely, h_2, T_2, v_2, M_2, s_2, and ρ_2. The normal shock wave conservation equations of Sec. 3.2 can then be numerically solved to obtain the free-stream values at location 1. This is the most direct solution path; however it is numerically demanding. Another solution path was chosen for this work, taking advantage of the gas dynamics theory of the Fanno-Rayleigh lines method (Ref 29).

The Fanno line results from the simultaneous solution of mass and energy conservation (Eq 11 and 13) while the Rayleigh line results from the simultaneous solution of mass and momentum conservation (Eq 11 and 12) (Ref 29). Their intersections on a Mollier diagram represent both sides of the shock wave (i.e., at these two points, the conservation Eq 11, 12, and 13 are all obeyed), as shown in Fig. 9. The two solutions are distinguished using the Second Law of Thermodynamics. In this way, the Fanno and Rayleigh supersonic branch intersection brings the values for h_1 and s_1, the enthalpy and entropy of the free-stream plasma jet before the shock wave. The value of the pressure p_1 is deduced since h_1 and s_1 are both function of pressure, and all other properties of the free-stream plasma jet can be calculated (T_1, v_1, M_1, and ρ_1).

3.3.1 Plasma Properties. To solve the conservation laws through the normal shock wave and to infer state 2 from state o2, the evaluation of the plasma properties is required. The argon plasma properties are obtained using data derived from argon partition functions (Ref 35) and the following assumptions:

- The quasi-neutral plasma is pure argon between 1,000 K and 20,000 K;

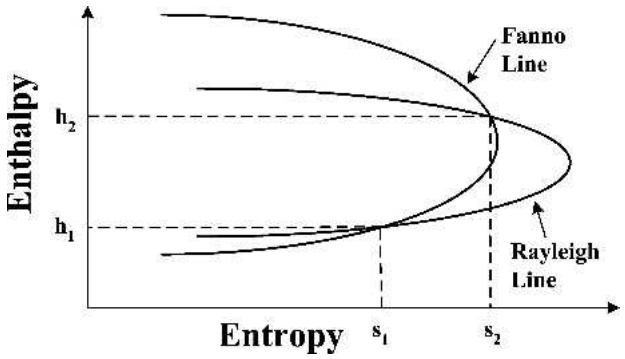

Fig. 9 Mollier diagram for the solution of the normal shock equations using the Fanno-Rayleigh lines technique

- The perfect gases law is obeyed;
- Only the first ionization of the argon plasma is considered through the three-body recombination:

$$\mathrm{Ar} + e^- \overset{K_{eq}}{\leftrightarrow} \mathrm{Ar}^+ + e^- + e^-$$

  where K_{eq} is the equilibrium constant (Ref 36);
- The argon plasma is in local thermodynamic equilibrium (LTE) (Ref 37).

4. Experimental Work

In this section the enthalpy probe and PSSPP measurements carried out for this work are presented.

4.1 Experimental Setup

The experimental setup includes a vacuum chamber, a pumping unit, a dc plasma torch installation, an enthalpy probe system, and a CCD camera, as shown in Fig. 10.

The plasma generation system was a Multicoat industrial installation from Sulzer-Metco Switzerland AG (Wohlen, Switzerland) for VPS composed of a dc plasma torch inside a water-cooled vacuum chamber. This chamber was implemented with a two-axis displacement system on which was mounted the plasma torch. It allowed the torch to move along and perpendicular to its axis (Ref 31, 33). A 12-bit CCD-camera with a zoom lens was also mounted on the vacuum chamber, facilitating the alignment of the torch with the enthalpy probe and the visualization of the plasma jet. Further details about the camera can be found in Ref 31.

The dc plasma torch was an F4-VB plasma gun from Sulzer-Metco, made of a copper anode with tungsten insert (6/12 mm throat/exit diameters) and a thoriated tungsten cathode. The plasma gas flowing around the cathode entered through a 16-hole helicoidal injector with 45° injection angle (Ref 31, 33).

The pumping unit was a Roots Vacuum Pumping Station WWD5500 from Pfeiffer Vacuum Technology AG (Asslar, Germany). It is composed of three major pieces: two roots pumps (WKP6000 and WKP1000) and a rotary vane pump (PAC400). With this pumping unit, it is possible to reach pressures as low as 10^{-2} Pa (no gas flowing); this lower limit rises to 50 Pa for 50 slpm argon flow rate (Ref 28, 31, 33). In fact, during operation the chamber pressure can be regulated between 10^2 and 5×10^4 Pa independent of the gas flow rate.

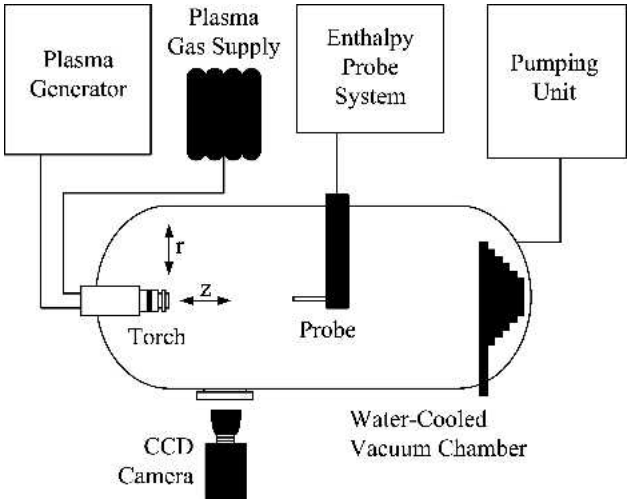

Fig. 10 Experimental setup for enthalpy probe and PSSPP measurements

The enthalpy probe system supplied by Tekna Plasma Systems (Sherbrooke, Québec, Canada) was designed to work at atmospheric pressure. Modifications were made to operate this equipment at lower pressures, noticeably the addition of a root pump for gas sampling and of specific pressure and gas flow rate measuring devices (Ref 31).

4.1.1 Operating Conditions. The enthalpy probe and PSSPP measurements were made while operating the system under the following conditions: pure argon flow rate of $Q_{Ar} = 40$ slpm, plasma torch current of $I = 400$ A (yielding 14 kW torch power), and chamber pressure of $p_c = 4000$ Pa.

For these operating conditions with nozzle dimensions of 6/12 mm throat/exit diameters, the torch exit pressure was measured as $p_e \approx 3300$ Pa and the supersonic plasma jet was overexpanded. Axial measurements were carried out to obtain the most salient features of this supersonic plasma jet in aerodynamic nonequilibrium.

4.1.2 Enthalpy Probe Measurements. The enthalpy probe had a 4.76 mm outer diameter (od) and a 1.5 mm inner diameter (id) and was covered with a TBC. With it mounted on the enthalpy probe system, the stagnation pressure p_{o2} was measured in tare mode while the stagnation enthalpy h_{o2} was obtained by comparing the heat fluxes from the tare and sample modes. The sensitivity of the enthalpy probe technique is linked with the amount of gas collected (Ref 38). In general, the larger the sampling rate, the better the enthalpy probe measurements (Ref 27). With a chamber pressure of 4000 Pa, the smallest probe available could not be used; the sampling rate was too low, rendering enthalpy measurements unsatisfactory. Yet the size of the enthalpy probe must not be too large, since it would lead to a reduced spatial resolution (i.e., swallowing the probe of section 2). Hence the present work deals with operating conditions close to the limit of applicability of the enthalpy probe method, requiring a certain trade-off on the localness of the measurements to insure the heat load difference is large enough to obtain the plasma enthalpy.

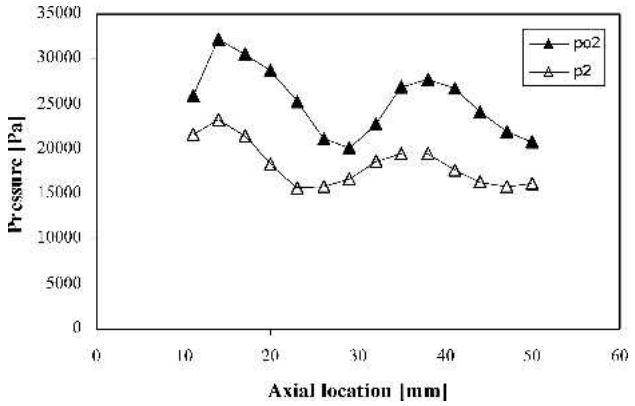

Fig. 11 Measured stagnation and static pressures along jet axis

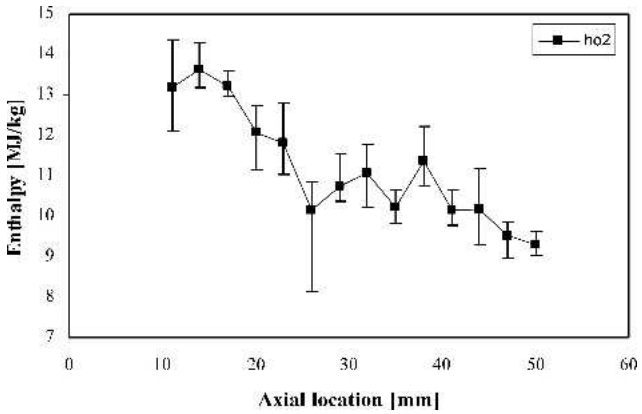

Fig. 12 Measured stagnation enthalpy along jet axis (note: ordinate scale starts at 7 MJ/kg)

The p_{o2} axial profile is presented in Fig. 11 (the error bars are not shown as they are worth less than one percent and would not appear due to the scale of the graph). As the jet is overexpanded, the flow exiting the plasma torch encounters shock waves that reduce its velocity. Consequently an increase in pressure is expected, with the stagnation pressure always larger than the static pressure (i.e., the former is related to zero velocity). The aerodynamic nonequilibrium state of the plasma jet causes oscillations of the p_{o2} axial profile. These oscillations have decreasing intensity along the axis as the jet spreads in the chamber and energy is dissipated at its fringes. All the preceding features are found in Fig. 11.

The h_{o2} axial profile is shown in Fig. 12 with the associated error bars showing a mean error over all locations around 6%. It is expected to decrease with axial locations downstream of the nozzle exit since the jet spreads into the chamber with reducing velocity from viscous effects. Again the aerodynamic nonequilibrium state of the LPPS jet causes oscillations of all the plasma properties. The intensity of these oscillations is linked with the magnitude of the pressure ratio p_1/p_c, which reduces from increasing viscous effects with axial location until it vanishes far from nozzle exit. Thus, Fig. 12 shows the smooth decrease expected on jet axis from spreading of the plasma jet.

The aerodynamic nonequilibrium state of the flow causes alternating compression and expansion regions that modify the shape of the supersonic plasma jet. Therefore, radial enthalpy probe measurements could be used to evaluate the energy conservation inside the jet and better assess the shape of the h_{o2} profile.

4.1.3 PSSPP Measurements. The PSSPP measurements were carried out using a 10 mm od enthalpy probe. This probe had a 5 mm id and was covered with a TBC. The 6 mm od PSSPP was inserted at the tip of the enthalpy probe to measure the static pressure p_2.

The p_2 axial profile is presented in Fig. 11. Similar to the p_{o2} profile, it is first expected to increase as the flow exiting the torch travels through shock waves. Oscillations result from the aerodynamic nonequilibrium state of the jet; their intensity decreases along jet axis from energy dissipation and spreading of the jet. These trends are all found in Fig. 11.

Combining PSSPP and enthalpy probe measurements, evidence that the plasma jet is overexpanded is to be found from the p_2 and p_{o2} pressure distributions. It should be bear in mind that the measurements correspond to subsonic values (i.e., after the tool-induced shock) from which must be deduced the trends of the supersonic values (i.e., before the shock). Using Eq 5, it is seen that a small p_{o2}/p_2 value corresponds to a small Mach number (M_2) while a larger value of p_{o2}/p_2 corresponds to a larger M_2. The M_2 values are to be linked with the normal shock wave process: the larger the Mach number of a supersonic flow (M_1), the stronger the shock wave and the smaller the Mach number of the ensuing subsonic flow (M_2). Therefore, in Fig. 13, it is seen that the flow goes through a compression zone first as p_{o2}/p_2 increases from the plasma torch exit to reach a maximum at $z \approx$ 20 mm, evidence that $p_e < p_c$. In other words, the increasing trend of p_{o2}/p_2 from torch exit tells that the shock process is weakening; thus a weaker shock is linked with a compression process and the jet is indeed overexpanded.

5. Results and Discussion

In this section, experimental results from Section 4 are used along with the new method to obtain the free-stream plasma jet characteristics.

The supersonic plasma jet is overexpanded, and alternating compression and expansion waves develop to bring the jet static pressure back to the chamber pressure. With compression waves, the flow is slowed down, raising its temperature and pressure, which in turn increase density and radiative losses. Conversely, opposite physical phenomena are observed for expansion waves: the flow accelerates and its temperature and pressure decrease, leading to lower density and radiative losses.

Figure 14 gives insight on the mechanisms taking place in an overexpanded jet. At the exit plane of the plasma torch nozzle, oblique shocks are formed that increase the jet static pressure (p) to reach the chamber pressure (p_c). These oblique shocks meet on the jet axis and are reflected away, creating a compression cell where p is larger than p_c. Meeting the jet boundaries, the oblique shocks are reflected as a series of expansion waves to bring p back at p_c. These expansion waves are then reflected on the jet axis, creating an expansion cell where p decreases under p_c. Reaching the jet boundaries, the expansion waves are reflected as compression waves that might coalesce to form oblique shocks and the compression/expansion pattern is repeated,

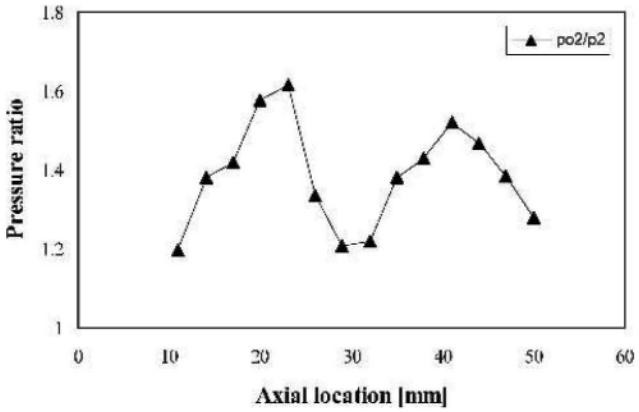

Fig. 13 Measured stagnation pressure/static pressure ratio along jet axis

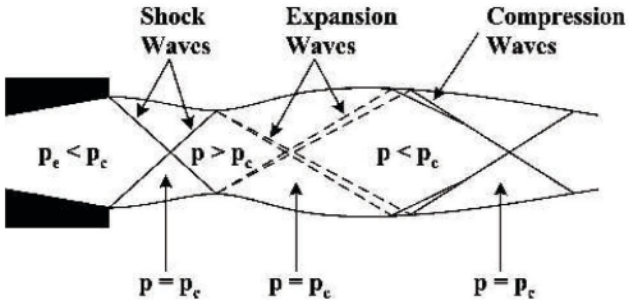

Fig. 14 Compression-expansion wave pattern in an overexpanded plasma jet

as illustrated in Fig. 3. Each repetition of this pattern comes along with an attenuation of the pressure changes due to viscous effects at the jet boundaries until p finally reaches p_c.

Figures 15-20 are used to analyze the solution obtained with the new method. They present a picture of the supersonic plasma jet (Fig. 15) and the axial profiles of salient flow properties on both side of the tool-induced shock wave, namely the static pressure (Fig. 16), the temperature (Fig. 17), the enthalpy (Fig. 18), the velocity (Fig. 19), and the Mach number (Fig. 20). From these figures, four qualitative fundamental observations can be made confirming the validity of the solution:

- The static pressure, the enthalpy and the temperature before the shock (p_1, h_1, T_1) are always smaller than the corresponding static pressure, enthalpy and temperature after the shock (p_2, h_2, T_2).
- The Mach numbers before the shock are greater than unity ($M_1 > 1$) while the Mach numbers after the shock are smaller than unity ($M_2 < 1$).
- All the plasma jet variables oscillate with decreasing intensity along the jet axis.
- The axial static pressure p_1 attains values three times as high as p_c in the first compression zone and values as low as p_c in the first expansion zone.

The first two observations confirm that the solution complies with the particular characteristics of a normal shock wave process and are supported by the qualitative agreement of the solution (trends from Fig. 16-20) with Fig. 15. The third observation shows that the supersonic plasma jet is in aerodynamic nonequilibrium from the presence of oscillations while the fourth is an indication of the invalidity of the $p_1 = p_c$ assumption. This last comment further demonstrates that the obtained p_1 axial distribution agrees with the theoretical jet behavior described in Fig. 14. The errors on the free-stream values of Fig. 16-20 result from the error involved in the stagnation enthalpy measurements (h_{o2}) since the pressure distributions p_{o2} and p_2 carry small errors. The larger influence is found on the enthalpy h_1 with error extending in average at ±8%. The other inferred values encounter much smaller fluctuations from the experimental error as the error represent an average of ±4% on the pressure p_1 and approximately

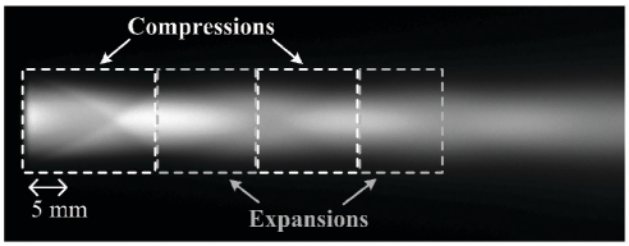

Fig. 15 Image of the overexpanded plasma jet for the chosen operating conditions (4000 Pa, 40 slpm Ar and 400 A)

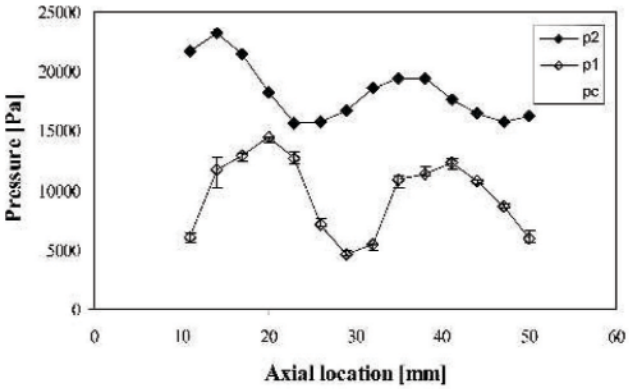

Fig. 16 Static pressure distributions on both sides of the induced shock wave along jet axis

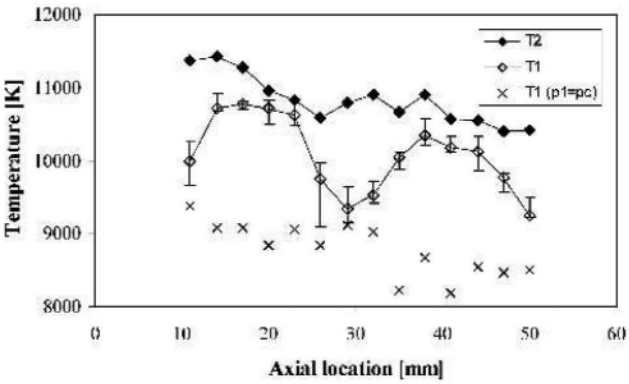

Fig. 17 Temperature distributions on both sides of the induced shock wave along jet axis (note: ordinate scale starts at 8000 K)

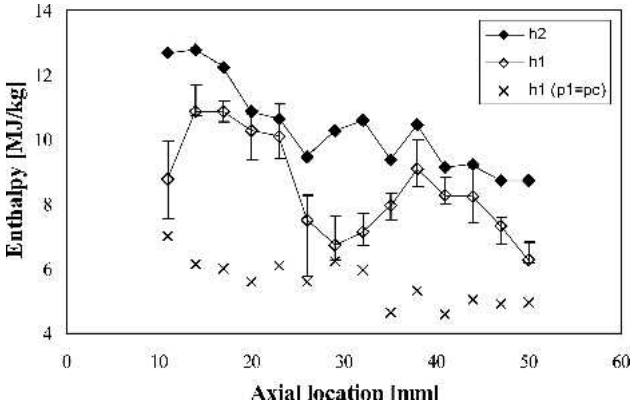

Fig. 18 Enthalpy distributions on both sides of the induced shock wave along jet axis (note: ordinate scale starts at 4 MJ/kg)

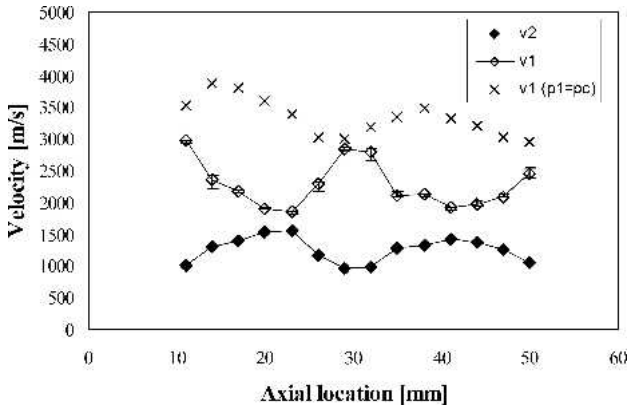

Fig. 19 Velocity distributions on both sides of the induced shock wave along jet axis

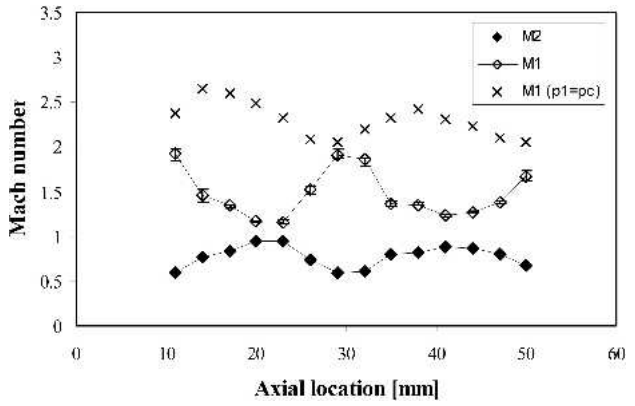

Fig. 20 Mach number distributions on both sides of the induced shock wave along jet axis

±2% for the velocity v_1, the Mach number M_1, and the temperature T_1. Such error values are acceptable and give an appreciation of the quality of the new method proposed in this work, which goes beyond respecting the behavior of jets in aerodynamic nonequilibrium.

From Fig. 14, the compression and expansion regions inside the overexpanded jet can be located in Fig. 15. Each region (compression or expansion) is composed of two zones due to the wave reflection on the jet axis, which creates a crossed pattern inside the jet.[3] These crossed patterns are surrounded by dashed boxes to illustrate both compression and expansion regions. Compression regions comprise two zones: the first has a pressure $p < p_c$ since it is located inside an expansion cell while in the second zone the pressure $p > p_c$ as the flow crosses compression waves, entering a compression cell. An opposite scenario applies for expansion regions (i.e., first zone in a compression cell, second zone in an expansion cell).

An overview of Fig. 15 and 16 shows that the first compression region inside the overexpanded jet spreads from torch exit ($z = 0$ mm) to $z \approx 20$ mm; the first measurement was taken at $z = 11$ mm. The first expansion region is found between 20 mm $< z <$ 30 mm. The second compression region extends between 30 mm $< z <$ 40 mm and is followed by the second expansion region between 40 mm $< z <$ 50 mm. Further downstream, it can be deduced from Fig. 3, 14, and 15 that turbulent mixing of the jet with stagnant gas in the chamber will bring the flow to subsonic speeds, and shock structures will not be seen anymore as p_1 will become closer to p_c.

Further details of the flow inside each region can be obtained from the trends of Fig. 16-20. As the flow aerodynamic nonequilibrium state is driven by the jet exit pressure, the analysis must start from the static pressure profile. Figure 16 shows the static pressure distributions (p_1 and p_2) on both sides of the tool-induced shock. The free-stream static pressure (p_1) first increases because the jet is overexpanded. It reaches a maximum after the shock waves cross on jet axis; at this point the free-stream flow is slower, inducing a weaker tool-induced shock causing a small pressure rise. Therefore around this axial location, p_1 and p_2 are close to one another. Conversely, when the flow crosses expansion waves, as happens around $z \approx 30$ mm, the flow velocity is larger and the tool-induced shock is stronger, causing a larger pressure increase. Hence at this location p_1 and p_2 are far apart from one another. It should also be pointed out that in the first expansion region ($z \approx 30$ mm), the pressure reaches p_c as required from Fig. 3 and 14.

Figures 17 and 18 show the temperature (T_1 and T_2) and enthalpy (h_1 and h_2) of the plasma jet on both sides of the tool-induced shock where salient physical features are linked with the compression and expansion phenomena previously described. As the plasma jet undergoes compression first, higher T_1 and h_1 values are encountered around $z \approx 20$ mm. The weaker tool-induced shock associated with compression waves brings T_1 and h_1 closer to T_2 and h_2 than the stronger tool-induced shock associated with expansion waves, and therefore when the flow is expanding T_1 and h_1 are far apart from T_2 and h_2.

From Fig. 19 and 20 are seen the velocity and Mach number distributions (respectively v_1, v_2, and M_1, M_2) behavior on jet axis. Again the values for the free-stream velocity and Mach

[3]In this work, the words cell, region, and zone refer to specific divisions of the overexpanded plasma jet: in a cell, the pressure trend is constant (i.e., larger or smaller than p_c) while a region is described with the dashed boxes of Fig. 15 and is composed of two zones located before and after the waves cross on jet axis.

number, v_1 and M_1, are closer to the values of v_2 and M_2 when the flow undergoes compression.

As seen from Fig. 16, the offset between p_1 and p_c is larger in compression zones where p_1 can be three times greater than p_c. Calculations were carried out using the technique outlined in Sec. 2.5.1 and yielded values for the free-stream temperature T_1, enthalpy h_1, velocity v_1, and Mach number M_1 at a static pressure of p_c. The obtained values are indicate by the X's in Fig. 16-20, which show an under-prediction for the values of temperature and enthalpy and an over-prediction for the values of velocity and Mach number. From these results, it is clear that the $p_1 = p_c$ assumption is not valid and should be rejected when dealing with a plasma jet in aerodynamic nonequilibrium.

5.1 Limitations

The low-pressure environment brings unavoidable interrogations about the LTE state of the plasma jet. Effectively, under such pressure conditions, fewer collisions inside the ionized gas lead to different temperature distributions for the electrons and heavy (i.e., atoms and ions) particles. A plasma jet in the non-LTE state could not be diagnosed with either the new method in the form developed so far or with regular enthalpy probe measurements, as the two temperature distributions (i.e., T_h and T_e) would be unknown. However, if LTE zones would exist and could be detected inside a non-LTE plasma jet, the new method would still be a valuable diagnostic tool. Favorable zones for LTE could be the compression regions where higher pressure and temperature multiply the number of collisions in the ionized gas for $T_e \approx T_h$. It should be understood that for a slight departure from LTE, the new method may be used with care and discernment.

The present PSSPP design is not yet optimal. An improvement would be to build a one-piece PSSPP; that is an enthalpy probe with no hole at its tip but rather an off-axis pressure tap to monitor static pressure. This would ensure cooling-off the tip, since for now the tungsten-made PSSPP is sustaining a high heat flux as shown by its bright reemission under plasma conditions. It would also enable the use of the PSSPP technique under higher chamber pressures or with binary gas mixtures since both of these operating conditions increase the heat flux to the PSSPP. A one-piece PSSPP would eliminate the joint between the PSSPP and the probe, where leaking can occur after several runs when both the PSSPP and the probe contact surfaces become worn, threatening the quality of the measurements.

Another limitation of the PSSPP is linked with the tap measurement distance d held constant in this work. This localization of the tap is determined by the reacceleration pattern of the plasma jet impinging on the PSSPP and should be varied depending on the plasma zone under study. Based on the modeling work, it is expected that the tap measurement distance should not change by more than a few percent.

6. Conclusions

The new method developed in this work fills a need for understanding supersonic plasma jets in aerodynamic nonequilibrium. Its major outcome is to provide physically meaningful free-stream supersonic plasma jet descriptions, improving the diagnostics over previous researches. The aerodynamic nonequilibrium features of the overexpanded plasma jet are taken into account considering the possible variation of p_1, avoiding the usual assumptions of aerodynamic equilibrium ($p_1 = p_c$) and calorically perfect gas (γ = constant). The principal influence of aerodynamic nonequilibrium is an oscillating static pressure distribution of the flow (i.e., $p_1 \neq p_c$) that results in oscillating velocity and temperature fields from compression and expansion waves in the jet. Consequently, the aerodynamic equilibrium assumption is clearly wrong, while the calorically perfect assumption has a lesser impact on the results for the operating conditions chosen in this work.

The improved diagnosis of the supersonic plasma jet is achieved using a new device (PSSPP) to gain access to an additional physical quantity, the static pressure behind the induced shock in the supersonic plasma jet. This device has a relatively short lifespan as it endures large heat flux inside the supersonic plasma jet. It is doubtful that the present design could sustain the increase in heat flux that would arise by either raising the chamber pressure or adding a secondary plasma gas. There is, however, no theoretical reason to limit the application of the new method to LPPS; it could be used for any supersonic plasma jet in aerodynamic nonequilibrium. Therefore, the requirement is obtaining a PSSPP design with the ability to sustain different conditions of chamber pressure and different mixtures of gases. For such a task, the one-piece PSSPP discussed in Sec. 5.1 could be a solution, and if a mixture of gases is used, a mass spectrometer must be implemented with the enthalpy probe system for the determination of composition. Still, the new method could also be improved by the inclusion of the radiative energy losses for the stagnation process (state 2 $\rightarrow$ o2) when subsonic values are inferred from stagnation measurements.

The major limitation of this work is its dependence towards LTE (or close-to-LTE) supersonic plasma jets. Extending the new method to a non-LTE description (two temperatures model) would require extra measurements for the species in the plasma. Yet as discussed in Sec. 5.1, a deep understanding of gas dynamics could lead to use of the new method in certain zones where LTE could be expected.

References

1. P. Fauchais and M. Vardelle, Plasma Spraying: Present and Future, *Pure Appl. Chem.,* Vol 66 (No. 6), 1994, p 1247-1258
2. R.W. Smith and R. Novak, Thermal Spraying: Advances and Applications in US Thermal Spray Technology I. Technology and Materials, *Powder Metall. Int.,* Vol 23 (No. 3), 1991, p 147-155
3. E. Pfender, Thermal Plasma Technology: Where Do We Stand and Where Are We Going?, *Plasma Chem. Plasma P.,* Vol 19 (No. 1), 1999, p 1-31
4. P. Fauchais, A. Vardelle, and B. Dussoubs, Quo Vadis Thermal Spraying?, *J. Therm. Spray Technol.,* 10(1), 2001, p 44-66
5. P. Fauchais and A. Vardelle, Thermal Plasmas, *IEEE T. Plasma Sci.,* Vol 25 (No. 6), 1997, p 1258-1280
6. P. Fauchais, Thermal Plasma Engineering Today in Western Europe, *High Temp. Chem. Proc.,* Vol 1, 1992, p 1-43
7. L. Prandtl, *Essential of Fluid Dynamics,* Hafner Publishing Company, New York, NY, 1952, 452 p 268
8. P.J. Meyer and D. Hawley, Electro-Plasma Inc. LPPS Production Systems, *Thermal Spray Coatings: Properties, Processes and Applications,* T.F. Benecki, Ed., May 4-10, 1991 (Pittsburgh, PA), ASM International, 1992, p 29-38
9. J. Grey, Thermodynamic Methods of High-Temperature Measurement, *ISA T.,* Vol 4 (No. 2), 1965, p 102-115

10. J. Grey, P.F. Jacobs, and M.P. Sherman, Calorimetric Probe for the Measurement of Extremely High Temperatures, *Rev. Sci. Instrum.,* Vol 33 (No. 7), 1962, p 738-741
11. S. Katta, J.A. Lewis, and W.H. Gauvin, A Plasma Calorimetric Probe, *Rev. Sci. Instrum.,* Vol 44 (No. 10), 1973, p 1519-1523
12. F.A. Vassallo, "Miniature Enthalpy Probes for High Temperature Gas Streams," Aerospace Research Laboratories (USAF), Paper ARL 66-0115, Wright-Patterson Air Force Base, OH, 1966.
13. F.J. Huber, "Probes for Measuring Mass Flux, Stagnation Point Heating, and Total Enthalpy of High Temperature Hypersonic Gas Flows," AIAA Aerodynamic Testing Conference, AIAA Paper No. 66-750, Los Angeles, CA, Sept 1966
14. F.A. Vassallo, "A Fast Acting Miniature Enthalpy Probe, AIAA Aerodynamic Testing Conference," AIAA Paper No.68-391, San Francisco, CA, April 1968
15. J. Grey and P.F. Jacobs, Experiments on Turbulent Mixing in a Partially Ionized Gas, *AIAA J.,* Vol 2 (No. 3), 1964, p 433-438
16. J. Grey, M.P, Sherman, P.M. Williams, and D.B. Fradkin, Laminar Arcjet Mixing and Heat Transfer: Theory and Experiments, *AIAA J.,* Vol 4 (No. 6), 1965, p 986-993
17. T.J. O'Connor, E.H. Comfort, and L.A. Cass, Turbulent Mixing of an Axisymmetric Jet of Partially Dissociated Nitrogen with Ambient Air, *AIAA J.,* Vol 4 (No. 11), 1966, p 2026-2032
18. L.A. Anderson and R.E. Sheldahl, Experiments with Two Flow-Swallowing Enthalpy Probes in High-Energy Supersonic Streams, *AIAA J.,* Vol 9 (No. 9), 1971, p 1804-1810
19. M. Brossa and E. Pfender, Probe Measurements in Thermal Plasma Jets, *Plasma Chem. Plasma P.,* Vol 8 (No. 1), 1988, p 75-90
20. E. Pfender, J.R. Fincke, and R. Spores, Entrainment of Cold Gas into Thermal Plasma Jets, *Plasma Chem. Plasma P.,* Vol 11 (No. 4), 1991, p 529-543
21. A. Capetti and E. Pfender, Probe Measurements in Argon Plasma Jets Operated in Ambient Argon, *Plasma Chem. Plasma P.,* Vol 9 (No. 2), 1989, p 329-341
22. W.D. Swank, J.R. Fincke, and D.C. Haggard, Modular Enthalpy Probe and Gas Analyzer for Thermal Plasma Measurements, *Rev. Sci. Instrum.,* Vol 64 (No. 1), 1993, p 56-62
23. J.R. Fincke, C.H. Chang, W.D. Swank, and D.C. Haggard, Entrainment and Demixing in Subsonic Thermal Plasma Jets: Comparison of Measurements and Predictions, *Int. J. Heat Mass Tran.,* Vol 37, 1994, p 1673-1682
24. J.R. Fincke, W.D. Swank, S.C. Snyder, and D.C. Haggard, Enthalpy Probe Performance in Compressible Thermal Plasma Jets, *Rev. Sci. Instrum.,* Vol 64 (No. 12), 1993, p 3585-3593
25. M. Hollenstein, M. Rahmane, and M.I. Boulos, Aerodynamic Study of the Supersonic Induction Plasma Jet, M. Hrabovský, M. Konrád, and V. Kopecký, Ed., *Organizing Committee of the 14th International Symposium on Plasma Chemistry,* Prague, Czech Republic, 1999, p 257-261
26. J.R. Fincke, S.C. Snyder, and W.D. Swank, Comparison of Enthalpy Probe and Laser Light Scattering Measurement of Thermal Plasma Temperatures and Velocities, *Rev. Sci. Instrum.,* Vol 64 (No. 3), 1993, p 711-718
27. M. Rahmane, G. Soucy, and M.I. Boulos, Analysis of the Enthalpy Probe Technique for Thermal Plasma Diagnostics, *Rev. Sci. Instrum.,* Vol 66 (No. 6), 1995, p 3424-3431
28. J.-L. Dorier, M. Gindrat, C. Hollenstein, M. Loch, A. Refke, A. Salito, and G. Barbezat, Plasma Jet Properties in a New Spraying Process at Low Pressure for Large Area Thin Film Deposition, *Thermal Spray 2001: New Surfaces for a New Millenium,* C.C. Berndt, K.A. Khor, and E.F. Lugscheider, Ed., May 28-30, 2001 (Singapore), ASM International, 2001, p 759-764
29. A.H. Shapiro, *The Dynamics and Thermodynamics of Compressible Fluid Flow,* John Wiley & Sons, New York, NY, 1953, 647, p 76-115
30. R. Henne, M. Müller, E. Proβ, G. Schiller, F. Gitzhofer, and M.I. Boulos, Near-Net-Shape Forming of Metallic Bipolar Plates for Planar Solid Oxide Fuel Cells by Induction Plasma Spraying, *J. Therm. Spray Technol.,* Vol 8 (No. 1), 1999, p 110-116
31. M. Gindrat, J-L. Dorier, C. Hollenstein, M. Loch, A. Refke, A. Salito, and G. Barbezat, Effect of Specific Operating Conditions on the Properties of LPPS Plasma Jets Expanding at Low Pressure, *International Thermal Spray Conference,* E. Lugscheider and C.C. Berndt, Ed., May 4-6, 2002 (Düsseldorf, Germany), DVS Deutscher Verband für Schweißen, DVS-Verlag GmBH, 2002, p 459-464
32. B. Jodoin, M. Gindrat, J-L. Dorier, C. Hollenstein, M. Loch, and G. Barbezat, Modelling and Diagnostics of a Supersonic DC Plasma Jet Expanding at Low Pressure, *International Thermal Spray Conference,* E. Lugscheider and C.C. Berndt, Ed., May 4-6, 2002 (Düsseldorf, Germany), DVS Deutscher Verband für Schweißen, DVS-Verlag GmBH, 2002, p 716-720
33. J-L. Dorier, B. Jodoin, M. Gindrat, A. Blais, C. Hollenstein, and G. Barbezat, A Novel Approach to Interpret Enthalpy Probe Measurements in Low Pressure Supersonic Plasma Jets, R. D'Agostino, Ed., *Organizing Committee of the 16th International Symposium on Plasma Chemistry,* Taormina, Italy, 2003
34. Y. Bartosiewicz, P. Proulx, and Y. Mercadier, A Self-Consistent Two-Temperature Model for the Computation of Supersonic Argon Plasma Jets, *J. Phys. D App. Phys.,* Vol 35, 2002, p 2139-2148
35. A.B. Murphy and C.J. Arundell, Transport Coefficicents of Argon, Nitrogen, Oxygen, Argon-Nitrogen, and Argon-Oxygen Plasmas, *Plasma Chem. Plasma P.,* Vol 14 (No. 4), 1994, p 451-490
36. M.I. Hoffert and H. Lien, Quasi-One-Dimensional, Nonequilibrium Gas Dynamics of Partially Ionized Two-Temperature Argon, *Phys. Fluids,* Vol 10 (No. 8), 1967, p 1769-1776
37. E.P. Muntz, B.B. Hamel, and B.L. Maguire, Some Characteristics of Exhaust Plume Rarefaction, *AIAA J.,* Vol 8 (No. 9), 1970, p 1651-1658
38. J.Grey, Sensitivity Analysis for the Calorimetric Probe, *Rev. Sci. Instrum.,* Vol 34 (No. 8), 1963, p 857-859